

Direct Detection of Vector Dark Matter

Junji HISANO^{1,2}, Koji ISHIWATA³ Natsumi NAGATA^{1,4} and Masato YAMANAKA⁵

¹*Department of Physics, Nagoya University, Nagoya 464-8602, Japan*

²*Institute for the Physics and Mathematics of the Universe, University of Tokyo, Kashiwa 277-8568, Japan*

³*California Institute of Technology, Pasadena, CA 91125, USA*

⁴*Department of Physics, University of Tokyo, Tokyo 113-0033, Japan*

⁵*MISC, Kyoto Sangyo University, Kyoto 603-8555, Japan*

In this paper, we complete formulae for the elastic scattering cross section of general vector dark matter with nucleons in the direct detection at the leading order of the strong coupling constant α_s , assuming that the dark matter is composed of vector particles and interacts with heavy fermions with color charge as well as standard-model quark. As an application of our formulae, the direct detection of the first Kaluza-Klein photon in the minimal universal extra dimension model is discussed. It is found that the scattering cross section is larger than those in the previous works by up to a factor of ten.

§1. Introduction

Cosmological observations have established the existence of dark matter. Nowadays, the energy density of dark matter is precisely determined using the Wilkinson Microwave Anisotropy Probe (WMAP) satellite.¹⁾ The standard model of particle physics, however, can explain neither its existence nor its nature, which has been a mystery in particle physics and cosmology. The Weakly Interacting Massive Particles (WIMPs) in models beyond the standard model are a good candidate for dark matter. The relic abundance is naturally consistent with the cosmological observation if WIMPs have TeV-scale mass and they are thermally produced in the early universe. This is the so-called thermal relic scenario. In this scenario, the dark matter is originally nonrelativistic and acts as cold dark matter in the era of the structure formation of the universe. The leading candidate of WIMP dark matter is the lightest neutralino in the minimal supersymmetric standard model, which is a Majorana fermion. In addition, other models beyond the standard model at the TeV scale predict the existence of stable vector particles, such as the Kaluza-Klein (KK) photon^{2),3)} in the universal extra dimensions (UED)^{4),5)} and the T -odd heavy photon^{6)–8)} in the Littlest Higgs model with T -parity.^{9),10)}

Now, the WIMP dark matter scenario has been tested in collider and direct detection experiments. In the Large Hadron Collider (LHC), (pair) production of the WIMP dark matter with TeV-scale mass is expected. On the other hand, XENON100,¹¹⁾ which is the largest-volume detector ever, is in operation to detect it as scattering signals with nuclei on the earth. If the WIMP-scattering events are discovered and its properties are measured in the direct detection experiments, the measurements would be tested using the data that indicates dark matter production at the LHC.

With such recent progress on the experimental side, the theoretical prediction of dark matter signals must have better accuracy. The collider signatures of dark matter (such as in supersymmetric or UED models) have been intensively studied. On the other hand, the scattering cross section of dark matter with nuclei in the direct detection experiments has also been calculated more accurately. In recent works,^{(12),(13)} it was pointed out that a gluon-WIMP effective interaction is one of the leading contributors to the elastic scattering cross section, and it was also shown how to evaluate it precisely. (In those works, the results are shown for supersymmetric dark matter.) For the other models, in contrast, the gluon contribution and other leading terms are not taken into account correctly in the calculation of the scattering cross section^{(3),(14),(15)} for the UED model and⁽⁷⁾ for the Littlest Higgs model with T -parity).

In this paper, we assume that WIMP dark matter is composed of vector particles, and evaluate its elastic scattering cross section with nucleons, which is relevant to the direct detection experiments. Here, we consider the case in which vector dark matter interacts with standard-model quarks and exotic heavy fermions, which is a fundamental representation of $SU(3)_c$. As an application of our formulae, we discuss the direct detection of the first KK photon in the minimal universal extra dimension (MUED) model. We found that the spin-independent scattering cross section with a proton is increased by up to a factor of ten, compared with those in the previous works. We also show that the spin-independent scattering cross section of the KK photon with a proton ranges from about $3 \times 10^{-46} \text{cm}^2$ to $5 \times 10^{-48} \text{cm}^2$ on the parameter region with the thermal relic abundance consistent with the cosmological observations. Future direct detection experiments with ton-scale detectors might cover the range.

This paper is organized as follows. In the next section, we briefly review the formulation for the scattering cross section of general vector dark matter with nuclei. Next, in §3, we derive the effective Lagrangian describing the interaction of general vector dark matter with quarks and gluons in target nuclei. In §4, we review the MUED model and summarize the mass spectra of KK particles, and apply the formulae that are generally derived to the case of the first KK photon dark matter. Then, we numerically calculate the scattering cross section of the first KK photon dark matter with/without higher KK mode contributions, and discuss the significance of each effective operator. Section 5 is devoted to the conclusion.

§2. Formalism of cross section for vector dark matter

In this section, we formulate the elastic cross section of general vector dark matter with nuclei. The cross section is calculated in terms of effective coupling constants, which are given by coefficients of effective interactions of vector dark matter with light quarks ($q = u, d, s$) and gluons. To begin with, we write down all the effective interactions that are relevant to the scattering. In the derivation, we referred to reference.⁽¹⁶⁾

Since the scattering process is nonrelativistic, all the terms that depend on the velocities of dark matter particles and nuclei are subdominant in the velocity

expansion. Therefore, we neglect the operators suppressed by the velocities of the dark matter particles or nuclei in our study. Then, physical degrees of freedom of the vector field, which we denote as B_μ with the mass M , where we also assume a real field, are restricted to their spatial components since $\partial_\mu B^\mu = 0$. As a consequence, in the expansion of a strong coupling constant and in the nonrelativistic limit of the scattering process, the leading interaction of the vector field with quarks and gluons is given as

$$\mathcal{L}^{\text{eff}} = \sum_{q=u,d,s} \mathcal{L}_q^{\text{eff}} + \mathcal{L}_G^{\text{eff}}, \quad (2.1)$$

with

$$\mathcal{L}_q^{\text{eff}} = f_q^m m_q B^\mu B_\mu \bar{q}q + f_q^{i\mathcal{D}} B^\mu B_\mu \bar{q}i\mathcal{D}q + \frac{d_q}{M} \epsilon_{\mu\nu\rho\sigma} B^\mu i\partial^\nu B^\rho \bar{q}\gamma^\sigma \gamma^5 q + \frac{g_q}{M^2} B^\rho i\partial^\mu i\partial^\nu B_\rho \mathcal{O}_{\mu\nu}^q, \quad (2.2)$$

$$\mathcal{L}_G^{\text{eff}} = f_G B^\rho B_\rho G^{a\mu\nu} G_{\mu\nu}^a + \frac{g_G}{M^2} B^\rho i\partial^\mu i\partial^\nu B_\rho \mathcal{O}_{\mu\nu}^g, \quad (2.3)$$

where m_q is the mass of a quark and $\epsilon^{\mu\nu\rho\sigma}$ is the totally antisymmetric tensor defined as $\epsilon^{0123} = +1$. Here, the covariant derivative is defined as $D_\mu \equiv \partial_\mu + ig_s A_\mu^a T_a$, with g_s , T_a , and A_μ^a being the $SU(3)_C$ coupling constant, generator, and the gluon field, respectively. $\mathcal{O}_{\mu\nu}^q$ and $\mathcal{O}_{\mu\nu}^g$ are the twist-2 operators (traceless parts of the energy-momentum tensor) for quarks and gluons, respectively,

$$\mathcal{O}_{\mu\nu}^q \equiv \frac{1}{2} \bar{q}i \left(D_\mu \gamma_\nu + D_\nu \gamma_\mu - \frac{1}{2} g_{\mu\nu} \mathcal{D} \right) q, \quad (2.4)$$

$$\mathcal{O}_{\mu\nu}^g \equiv \left(G_\mu^{a\rho} G_{\rho\nu}^a + \frac{1}{4} g_{\mu\nu} G_{\alpha\beta}^a G^{a\alpha\beta} \right). \quad (2.5)$$

Here, $G_{\mu\nu}^a$ is the field strength tensor of a gluon. In the derivation of the effective Lagrangian, we used the equations of motion for vector field, *i.e.*, $(\partial^2 - M^2)B_\mu = 0$. The third term in the right-hand side of Eq. (2.2) contributes to the spin-dependent interaction in the scattering of dark matter with nuclei, while the other terms in the effective Lagrangian contribute to the spin-independent one.

Scattering amplitude is given by the matrix element of the effective interaction put between initial and final states. In this evaluation, we use the equation of motion for light quarks. The validity of the application is proven in the case where the operator is evaluated using on-shell hadron states.¹⁷⁾ Then, denoting $|N\rangle$ ($N = p, n$) as the on-shell nucleon state, we can evaluate the second term in Eq. (2.2) as

$$\langle N | \bar{q}i\mathcal{D}q | N \rangle = \langle N | m_q \bar{q}q | N \rangle. \quad (2.6)$$

Now, let us first examine the spin-independent scattering. As in the scattering process, the momentum transfer is negligible; the matrix elements between initial and final nucleon states with the mass m_N ($N = p, n$) are obtained as

$$\begin{aligned} \langle N | m_q \bar{q}q | N \rangle / m_N &\equiv f_{Tq}, \\ 1 - \sum_{u,d,s} f_{Tq} &\equiv f_{TG}, \end{aligned}$$

$$\begin{aligned}
\langle N(p) | \mathcal{O}_{\mu\nu}^q | N(p) \rangle &= \frac{1}{m_N} (p_\mu p_\nu - \frac{1}{4} m_N^2 g_{\mu\nu}) (q(2) + \bar{q}(2)) , \\
\langle N(p) | \mathcal{O}_{\mu\nu}^g | N(p) \rangle &= \frac{1}{m_N} (p_\mu p_\nu - \frac{1}{4} m_N^2 g_{\mu\nu}) G(2) .
\end{aligned} \tag{2.7}$$

In the matrix elements of twist-2 operators, $q(2)$, $\bar{q}(2)$, and $G(2)$ are the second moments of the parton distribution functions (PDFs) of a quark $q(x)$, antiquark $\bar{q}(x)$ and gluon $g(x)$, respectively,

$$\begin{aligned}
q(2) + \bar{q}(2) &= \int_0^1 dx x [q(x) + \bar{q}(x)] , \\
G(2) &= \int_0^1 dx x g(x) .
\end{aligned} \tag{2.8}$$

Then, after the trivial calculation of matrix elements for vector dark matter states, we obtain a spin-independent effective coupling of vector dark matter with nucleons, f_N , as

$$\begin{aligned}
f_N/m_N &= \sum_{q=u,d,s} f_q f_{Tq} + \sum_{q=u,d,s,c,b} \frac{3}{4} (q(2) + \bar{q}(2)) g_q \\
&\quad - \frac{8\pi}{9\alpha_s} f_{TG} f_G + \frac{3}{4} G(2) g_G ,
\end{aligned} \tag{2.9}$$

where $f_q \equiv f_q^m + f_q^{i\mathcal{P}}$ and $\alpha_s = g_s^2/4\pi$. Note that the effective scalar coupling of dark matter with gluons, f_G , gives the leading contribution to the cross section even if it is suppressed by a one-loop factor compared with those of light quarks. On the other hand, the contributions with the twist-2 operators of gluons are of the next-leading order as g_G is suppressed by α_s . Thus, we ignore them in this paper.

The spin-dependent scattering can be dealt with in a similar manner; the spin-dependent effective coupling is given by

$$a_N = \sum_{q=u,d,s} d_q \Delta q_N , \tag{2.10}$$

with

$$2s_\mu \Delta q_N \equiv \langle N | \bar{q} \gamma_\mu \gamma_5 q | N \rangle , \tag{2.11}$$

where s_μ is the spin of a nucleon.

For our calculation, we describe, in Table I, the input parameters for the hadronic matrix elements that we use in this article. The mass fractions and spin fractions (in a proton) of light quarks, f_{Tq} and Δq_p , are evaluated using the results in Refs.^{18)–20)} and Ref.²¹⁾ respectively. The prescription for evaluating the mass fraction is described in these references and Ref.¹³⁾

The second moments of PDFs of gluons, quarks, and antiquarks in a proton, on the other hand, have scale dependence. We use the values that are calculated at the scale $\mu = m_Z$ (m_Z is Z boson mass). This is because all the terms (and

Table I. Parameters for quark and gluon matrix elements used in this paper. f_{Tq} are evaluated using the results in Refs.¹⁸⁾⁻²⁰⁾ The spin fractions for a proton are obtained from Ref.²¹⁾ The second moments of PDFs of gluons, quarks, and antiquarks in a proton are calculated at the scale $\mu = m_Z$ using the CTEQ parton distribution.²²⁾

For proton		Spin fraction (for proton)		Second moment at $\mu = m_Z$ (for proton)			
f_{Tu}	0.023			Δu_p	0.77	$G(2)$	0.48
f_{Td}	0.032	Δd_p	-0.49	$u(2)$	0.22	$\bar{d}(2)$	0.036
f_{Ts}	0.020	Δs_p	-0.15	$d(2)$	0.11	$\bar{s}(2)$	0.026
For neutron				$s(2)$	0.026	$\bar{c}(2)$	0.019
f_{Tu}	0.017			$c(2)$	0.019	$\bar{b}(2)$	0.012
f_{Td}	0.041			$b(2)$	0.012		
f_{Ts}	0.020						

coefficients) in effective couplings should be evaluated at the scale of the mass of the particle that mediates the scattering.^{*)} It is obvious at tree level scattering. Even in the case where the loop diagram induces scattering, it is understandable from the fact that the loop integration is dominated by the particle mass.^{**)} The numerical values of the second moments of PDFs are shown in Table I using the CTEQ parton distribution.²²⁾ The spin fractions and second moments for a neutron are given by the exchange of up and down quarks.

Eventually, using f_N and a_N , we express the elastic scattering cross section of vector dark matter with target nuclei as follows:

$$\sigma = \frac{1}{\pi} \left(\frac{m_A}{M + m_A} \right)^2 \left[|n_p f_p + n_n f_n|^2 + \frac{8}{3} \frac{J+1}{J} |a_p \langle S_p \rangle + a_n \langle S_n \rangle|^2 \right]. \quad (2.12)$$

Here, m_A is the mass of target nucleus A . n_p and n_n are proton and neutron numbers in the target nucleus, respectively, while J is the total spin of the target nucleus and $\langle S_N \rangle = \langle A | S_N | A \rangle$ are the expectation values of the total spin of protons and neutrons in A . The first term in the brackets on the right-hand side comes from the spin-independent interactions, while the second one is generated by the spin-dependent one.

^{*)} Here, some readers may concern about it by considering $1/Q^2$ (Q is momentum transfer) expansion in the operator-product expansion method, such as in the evaluation of the deep inelastic scattering cross section of hadrons. However, that is not what we are considering. Rather, we derive the effective Lagrangian in a similar manner to when one derives the weak-interaction Lagrangian at low energy from a fundamental theory. When one gives a theoretical prediction of physical observables from the weak-interaction effective Lagrangian, one should set a renormalization scale in the evaluation of the matrix element of the physical amplitude to the weak scale, *i.e.*, the mass scale of the particle that mediates the scattering, in order to make the theoretical prediction accurate without calculating higher order quantum corrections. This is why PDFs at the weak scale are a good approximation.

^{**)} We thank Mark B. Wise for pointing this out.

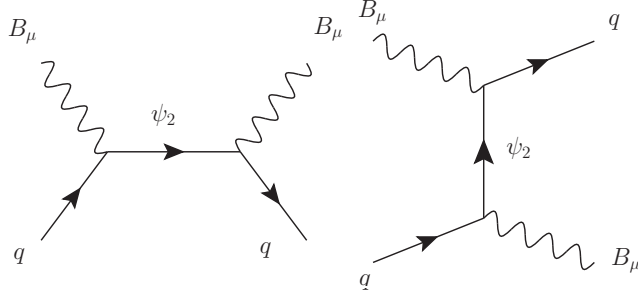


Fig. 1. Tree level diagrams of color triplet fermion ψ_2 exchange to generate interaction of vector dark matter with quarks.

§3. Effective Lagrangian

In this section, we derive the effective Lagrangian for general vector dark matter, which was introduced in the previous section. As we described in the Introduction, we assume that vector dark matter has interactions with fermions with color charge, in which quarks are included. Denoting these fermions as ψ_1 and ψ_2 with masses m_1 and m_2 , respectively, we start with a simply parametrized interaction Lagrangian of the form:

$$\mathcal{L} = \bar{\psi}_2 (a_{\psi_2\psi_1} \gamma^\mu + b_{\psi_2\psi_1} \gamma^\mu \gamma_5) \psi_1 B_\mu + \text{h.c.} \quad (3.1)$$

Here, we do not consider the case in which vector dark matter couples to a pair of quarks, since otherwise it would become unstable. We take $m_2 > m_1$ without loss of generality here and thereafter. We also assume, for simplicity, that ψ_1 and ψ_2 are color triplets. It is straightforward to extend to the other cases.

First, let us examine the scattering with quarks. The vector dark matter is scattered by quarks at the tree level. The relevant interaction Lagrangian is given by taking $\psi_1 = q$ in Eq. (3.1), and the diagrams are shown in Fig. 1. After integrating out the heavy particle ψ_2 , the coefficients in Eq. (2.2), *i.e.*, scalar-, axial-vector-, and twist-2-type couplings with quarks, are induced as follows:

$$f_q = \frac{a_{\psi_2q}^2 - b_{\psi_2q}^2}{m_q} \frac{m_2}{m_2^2 - M^2} - (a_{\psi_2q}^2 + b_{\psi_2q}^2) \frac{m_2^2}{2(m_2^2 - M^2)^2}, \quad (3.2)$$

$$d_q = \frac{iM(a_{\psi_2q}^2 + b_{\psi_2q}^2)}{m_2^2 - M^2}, \quad (3.3)$$

$$g_q = -\frac{2M^2(a_{\psi_2q}^2 + b_{\psi_2q}^2)}{(m_2^2 - M^2)^2}. \quad (3.4)$$

Here, we take the zero quark mass limit. As is obvious, the effective couplings obtained here are enhanced when the vector dark matter and the heavy colored fermion are degenerate in mass.

Next, let us discuss the interaction with gluons. The vector dark matter does not couple with gluons at the tree level; however, it does at the loop level, as shown

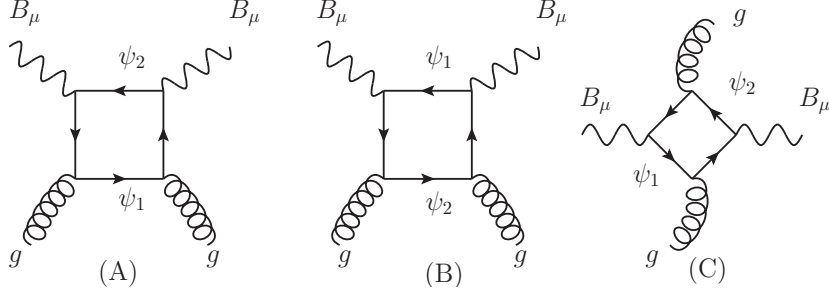


Fig. 2. One-loop contributions to scalar-type effective coupling with gluons.

in Fig. 2. In those loop level processes, all the heavy particles ψ_1 and ψ_2 that couple with B_μ contribute, in addition to quarks. The contribution of each diagram, (A), (B), and (C), to the scalar-type effective coupling with gluons f_G in Eq. (2·3) is written as

$$f_G^{(I)} = \frac{\alpha_s}{4\pi} \left[(a_{\psi_2\psi_1}^2 + b_{\psi_2\psi_1}^2) f_+^{(I)}(M; m_1, m_2) + (a_{\psi_2\psi_1}^2 - b_{\psi_2\psi_1}^2) f_-^{(I)}(M; m_1, m_2) \right], \quad (3\cdot5)$$

where $f_+^{(I)}$ and $f_-^{(I)}$ (I=A, B, and C) are given after the loop calculation,

$$\begin{aligned} f_+^{(A)}(M; m_1, m_2) &= \frac{1}{6\Delta^2 M^2} \left[\Delta [M^2(m_2^2 - m_1^2) + m_1^2(m_1^2 + 5m_2^2)] \right. \\ &\quad \left. - 6m_1^2 m_2^2 [(m_2^2 - m_1^2)^2 - M^2(m_1^2 + 3m_2^2)] \right] - \frac{m_1^2}{12M^4} \ln\left(\frac{m_1^2}{m_2^2}\right) \\ &+ \frac{m_1^2 L}{12\Delta^2 M^4} \left[(m_2^2 + m_1^2 - M^2)\Delta^2 + 2m_2^2 \Delta \{5m_2^4 + 20m_1^2 m_2^2 - m_1^4 + M^2(9m_2^2 + m_1^2)\} \right. \\ &\quad \left. + 12m_2^4 \{M^2(m_2^4 + 10m_1^2 m_2^2 + 5m_1^4) - (m_2^2 - m_1^2)^2(m_2^2 + 3m_1^2)\} \right], \quad (3\cdot6) \end{aligned}$$

$$\begin{aligned} f_-^{(A)}(M; m_1, m_2) &= -\frac{m_2}{6m_1 \Delta^2} \left[\Delta(2m_2^2 + m_1^2 - 2M^2) + 6m_1^2 m_2^2 (m_2^2 - m_1^2 - M^2) \right] \\ &\quad + \frac{m_1 m_2^3 \{ \Delta + m_1^2 (m_2^2 - m_1^2 + M^2) \}}{\Delta^2} L, \quad (3\cdot7) \end{aligned}$$

$$\begin{aligned} f_+^{(C)}(M; m_1, m_2) &= -\frac{2M^4 - 3(m_1^2 + m_2^2)M^2 + (m_1^2 - m_2^2)^2}{6\Delta M^2} \\ &\quad + \frac{m_1^2}{12M^4} \ln\left(\frac{m_1^2}{m_2^2}\right) + \frac{m_2^2}{12M^4} \ln\left(\frac{m_2^2}{m_1^2}\right) \\ &+ \frac{\Delta(M^2 - m_1^2 - m_2^2)(m_1^2 + m_2^2) + 4m_1^2 m_2^2 \{ (m_1^2 - m_2^2)^2 - 2M^2(m_1^2 + m_2^2) \}}{12\Delta M^4} L, \quad (3\cdot8) \end{aligned}$$

and

$$f_+^{(B)}(M; m_1, m_2) = f_+^{(A)}(M; m_2, m_1), \quad (3.9)$$

$$f_-^{(B)}(M; m_1, m_2) = f_-^{(A)}(M; m_2, m_1), \quad (3.10)$$

$$f_-^{(C)}(M; m_1, m_2) = 0. \quad (3.11)$$

Here, we defined functions Δ and L as

$$\Delta(M; m_1, m_2) \equiv M^4 - 2M^2(m_1^2 + m_2^2) + (m_2^2 - m_1^2)^2, \quad (3.12)$$

$$L(M; m_1, m_2) \equiv \begin{cases} \frac{1}{\sqrt{|\Delta|}} \ln \left(\frac{m_2^2 + m_1^2 - M^2 + \sqrt{|\Delta|}}{m_2^2 + m_1^2 - M^2 - \sqrt{|\Delta|}} \right) & (\Delta > 0) \\ \frac{2}{\sqrt{|\Delta|}} \tan^{-1} \left(\frac{\sqrt{|\Delta|}}{m_2^2 + m_1^2 - M^2} \right) & (\Delta < 0) \end{cases}. \quad (3.13)$$

The total scalar-type effective coupling with gluons is obtained by the summation of $f^{(I)}$ for $I = A, B$ and C . Here, one should be careful in dealing with the contribution of the diagrams in the case where ψ_1 is a quark. In such a case, there exist diagrams in which momentum with the scale of quark mass dominates the loop integral. We call them ‘‘long-distance’’ contributions. On the other hand, we describe the contributions from the diagrams in which the loop momentum with the scale of particle heavier than quarks dominates the integral as ‘‘short-distance’’ ones. When one derives the effective coupling in the three-flavour effective theory from the six-flavour full one, one should not include the contribution of light quarks in the long-distance diagrams, as discussed in Refs.^{12),13)} To identify the long-distance contribution among diagrams, let us consider the case where ψ_1 is a quark (*i.e.*, $m_q \ll m_2$). In this limit, the long-distance contribution in f_G should approach to $-\frac{\alpha_s}{12\pi} f_q$, which is obtained by the calculation of triangle diagrams for emitting two gluons using the scalar-type effective coupling with quarks in Eq. (3.2);²³⁾

$$f_+^{(A)}(M; m_q, m_2) \rightarrow \frac{m_2^2}{6(m_2^2 - M^2)^2}, \quad (3.14)$$

$$f_-^{(A)}(M; m_q, m_2) \rightarrow -\frac{m_2}{3m_q(m_2^2 - M^2)}, \quad (3.15)$$

$$f_+^{(B)}(M; m_q, m_2) \rightarrow \frac{m_2^2}{6(m_2^2 - M^2)M^2} + \frac{m_2^2}{6M^4} \ln \left(1 - \frac{M^2}{m_2^2} \right), \quad (3.16)$$

$$f_-^{(B)}(M; m_q, m_2) \rightarrow -\frac{m_q(m_2^2 - 2M^2)}{6m_2(m_2^2 - M^2)^2}, \quad (3.17)$$

$$f_+^{(C)}(M; m_q, m_2) \rightarrow \frac{1}{6(m_2^2 - M^2)} - \frac{1}{6M^2} - \frac{m_2^2}{6M^4} \ln \left(1 - \frac{M^2}{m_2^2} \right). \quad (3.18)$$

It is found that diagram (A) gives the long-distance contribution, whereas the others yield the short-distance ones. Therefore, f_G should be given as

$$f_G = \sum_{\psi_2, q=c, b, t} c_q f_G^{(A)} + \sum_{\psi_2, q=\text{all}} (f_G^{(B)} + f_G^{(C)}). \quad (3.19)$$

Here, $c_q = 1 + 11\alpha_s(m_q)/4\pi$ is the additional long-distance QCD correction pointed out in Ref.²⁴⁾ We evaluate it as $c_c = 1.32$ and $c_b = 1.19$ for $\alpha_s(m_Z) = 0.118$, and also adopt $c_t = 1$ for simplicity. On the other hand, if there are no quarks in the loop, all the diagrams indicate as short-distance contributions. In such a case, f_G is simply obtained as

$$f_G = \sum_{\psi_1, \psi_2} (f_G^{(A)} + f_G^{(B)} + f_G^{(C)}). \quad (3.20)$$

§4. Cross section of Kaluza-Klein dark matter with nucleons

In this section, we apply the above results to the evaluation for the direct detection of the lightest Kaluza-Klein particle (LKP) in a model with UED.^{4),5)} Among the variety of UED models, the MUED model, in which one extra dimension is compactified on an S^1/Z_2 orbifold and a dark matter candidate is included, is most extensively investigated.^{2),3)} In the MUED model, the stabilization of LKP is ensured by the KK parity conservation. It originates from the momentum conservation along the fifth-dimensional space. The KK parity -1 ($+1$) is assigned to particles with odd (even) KK number. This assignment and the KK parity conservation prevent the lightest KK-odd particle from decaying to the standard-model particles.

The mass spectra of KK particles including radiative corrections were calculated in Ref.⁵⁾ The work⁵⁾ found that the LKP was the first KK photon in the broad range on the MUED-model parameter space, and would be a dark matter candidate. The relic abundance of the first KK photon dark matter was precisely calculated.^{25)–28)} From those analyse, the compactification scale $1/R$ consistent with the cosmological observations is $600 \text{ GeV} \lesssim 1/R \lesssim 1400 \text{ GeV}$ and the standard-model Higgs boson mass is $m_h \lesssim 230 \text{ GeV}$. From the indirect low-energy experiments and corresponding analyses, which are $b \rightarrow s\gamma$,²⁹⁾ B meson decay,^{30)–32)} B^0 - \bar{B}^0 oscillation,³³⁾ and electroweak precision measurements,³⁴⁾ the lower bound on the compactification scale is obtained as $1/R \gtrsim 600 \text{ GeV}$. Thus, the favorable compactification scale in light of the relic abundance is free from experimental limits, and despite the simple framework, the MUED model is phenomenologically successful.

In the following, we assume the first KK photon to be the LKP and evaluate its elastic scattering cross section with nucleons, which is relevant to the direct detection of the LKP dark matter. At the beginning of this section, we explain the parametrization of the MUED model, and describe the mass spectra of KK particles. Then, we give the effective couplings of the LKP with quarks and gluons. Finally, the numerical results are shown.

4.1. Mass spectra of KK particles

First, we summarize the mass spectra of KK particles relevant to the direct detection of LKP dark matter. We employ the minimal particle contents, *i.e.*, gravitons and right-handed neutrinos are not included in this framework. Then, the first KK photon ($\gamma^{(1)}$) or the first KK charged Higgs boson ($H^{\pm(1)}$) becomes the LKP, depending on the compactification scale and standard-model Higgs boson mass. Since

the $H^{\pm(1)}$ dark matter scenario is excluded phenomenologically, we mainly study the parameter region where $\gamma^{(1)}$ is the LKP unless otherwise mentioned.

The mass of the first KK photon is obtained by diagonalizing the squared mass matrix for the first KK neutral gauge bosons,

$$\begin{pmatrix} (1/R)^2 + \delta m_{B^{(1)}}^2 + g_1^2 v^2/4 & g_1 g_2 v^2/4 \\ g_1 g_2 v^2/4 & (1/R)^2 + \delta m_{W^{(1)}}^2 + g_2^2 v^2/4 \end{pmatrix}. \quad (4.1)$$

This is written in a $(B^{(1)}, W^{3(1)})$ basis, where $B^{(1)}$ and $W^{3(1)}$ are the first KK particles of $U(1)_Y$ and $SU(2)_L$ gauge bosons, respectively. Here, g_1 (g_2) represents the $U(1)_Y$ ($SU(2)_L$) gauge coupling constant, and v ($\simeq 246$ GeV) is the vacuum expectation value of the standard-model Higgs boson. Radiative corrections, $\delta m_{B^{(1)}}^2$ and $\delta m_{W^{(1)}}^2$, were calculated in the work⁵⁾ as

$$\delta m_{B^{(1)}}^2 = -\frac{39}{2} \frac{g_1^2 \zeta(3)}{16\pi^4 R^2} - \frac{1}{6} \frac{g_1^2}{16\pi^2 R^2} \ln(\Lambda^2 R^2), \quad (4.2)$$

$$\delta m_{W^{(1)}}^2 = -\frac{5}{2} \frac{g_2^2 \zeta(3)}{16\pi^4 R^2} + \frac{15}{2} \frac{g_2^2}{16\pi^2 R^2} \ln(\Lambda^2 R^2). \quad (4.3)$$

Here, Λ is the ultraviolet cutoff scale of the UED model, which is ordinarily taken to be $\Lambda \sim \mathcal{O}(10/R)$.⁵⁾ ($\zeta(n)$ is Riemann's zeta function.) Since the off-diagonal component is so small in the mass matrix, the KK photon $\gamma^{(1)}$ is approximately identical to the weak eigenstate $B^{(1)}$. Therefore, we consider $B^{(1)}$ as the $\gamma^{(1)}$, and take the mass of the LKP equal to the mass of $B^{(1)}$. On the other hand, the mass of the first KK charged Higgs boson is given by

$$m_{H^{\pm(1)}}^2 = (1/R)^2 + m_W^2 + \delta m_{H^{\pm(1)}}^2, \quad (4.4)$$

$$\delta m_{H^{\pm(1)}}^2 = \left(\frac{3}{4} g_1^2 + \frac{3}{2} g_2^2 - \lambda_h \right) \frac{1}{16\pi^2 R^2} \ln(\Lambda^2 R^2). \quad (4.5)$$

Here, λ_h is the self-coupling constant of the standard-model Higgs boson, which is defined by $\lambda_h \equiv m_h^2/v^2$. When the standard-model Higgs boson is sufficiently heavy, the radiative correction $\delta m_{H^{\pm(1)}}^2$ gains a negative contribution so that the first KK charged Higgs boson is the LKP.

Next, we describe the mass spectra of KK quarks. They are important since most of the effective couplings of LKP dark matter with nucleons are very sensitive to the mass-square difference between the KK quarks and dark matter, which we will see later. The mass matrix of the n -th KK quarks is written in the weak eigenstate basis. The up-type quark mass matrix, for instance, is given by

$$- \begin{pmatrix} \bar{u}'^{(n)} & \bar{U}'^{(n)} \end{pmatrix} \begin{pmatrix} -m_{u1}^{(n)} & m_u \\ m_u & m_{u2}^{(n)} \end{pmatrix} \begin{pmatrix} u'^{(n)} \\ U'^{(n)} \end{pmatrix}, \quad (4.6)$$

where $u'^{(n)}$ and $U'^{(n)}$ describe the n -th KK modes associated with the $SU(2)_L$ singlet up-type quark and the up-type quark in the $SU(2)_L$ doublet, respectively, and m_u

is the mass of the (zero-mode, *i.e.*, standard-model) up-type quark. The down-type quark mass is written similarly. The parameters $m_{u1}^{(n)}$ and $m_{u2}^{(n)}$ are given as $m_{u1}^{(n)} = n/R + \delta m_{u(n)}$ and $m_{u2}^{(n)} = n/R + \delta m_{U(n)}$ with the radiative corrections:

$$\begin{aligned}\delta m_{u(n)} &= \left(3g_s^2 + g_1^2\right) \frac{n \ln(\Lambda^2 R^2)}{R \cdot 16\pi^2}, \\ \delta m_{U(n)} &= \left(3g_s^2 + \frac{27}{16}g_2^2 + \frac{1}{16}g_1^2\right) \frac{n \ln(\Lambda^2 R^2)}{R \cdot 16\pi^2}.\end{aligned}\quad (4.7)$$

On the other hand, the radiative corrections in the mass matrix of the n -th KK down-type quarks ($d'^{(n)}$ and $D'^{(n)}$ for $SU(2)_L$ singlet and in doublet, respectively) are

$$\begin{aligned}\delta m_{d(n)} &= \left(3g_s^2 + \frac{1}{4}g_1^2\right) \frac{n \ln(\Lambda^2 R^2)}{R \cdot 16\pi^2}, \\ \delta m_{D(n)} &= \delta m_{U(n)}.\end{aligned}\quad (4.8)$$

The equality in the latter comes from the fact that $D'^{(n)}$ and $U'^{(n)}$ make a $SU(2)_L$ doublet. In addition to these radiative corrections from gauge couplings, the third-generation KK quarks also receive the corrections from top Yukawa coupling y_t . They are given by

$$\begin{aligned}\delta_{y_t} m_{t(n)} &= \left(-\frac{3}{2}y_t^2\right) \frac{n \ln(\Lambda^2 R^2)}{R \cdot 16\pi^2}, \\ \delta_{y_t} m_{T(n)} = \delta_{y_t} m_{B(n)} &= \left(-\frac{3}{4}y_t^2\right) \frac{n \ln(\Lambda^2 R^2)}{R \cdot 16\pi^2},\end{aligned}\quad (4.9)$$

for the $SU(2)$ singlet and doublet, respectively. The mass eigenstates of the n -th KK quark modes are expressed in linear combinations of their weak eigenstates. For example, in the up-type quark sector, the relationship between the mass eigenstates (denoted as $u^{(n)}$ and $U^{(n)}$) and the weak eigenstates is expressed as follows:

$$\begin{pmatrix} u'^{(n)} \\ U'^{(n)} \end{pmatrix} = \begin{pmatrix} -\gamma_5 \cos \alpha^{(n)} & \sin \alpha^{(n)} \\ \gamma_5 \sin \alpha^{(n)} & \cos \alpha^{(n)} \end{pmatrix} \begin{pmatrix} u^{(n)} \\ U^{(n)} \end{pmatrix}.\quad (4.10)$$

Then, one obtains the mass eigenvalues from Eqs. (4.10) and (4.6) as

$$m_{u^{(n)}/U^{(n)}} = \sqrt{\left(\frac{m_{u1}^{(n)} + m_{u2}^{(n)}}{2}\right)^2 + m_u^2} \pm \frac{m_{u1}^{(n)} - m_{u2}^{(n)}}{2}\quad (4.11)$$

with the mixing angle

$$\sin 2\alpha_u^{(n)} = \frac{2m_u}{m_u^{(n)} + m_U^{(n)}}.\quad (4.12)$$

The off-diagonal component in Eq. (4.6) is small so that the mass eigenstates are approximately given by the weak ones and the mixing angle is tiny. However, the mixing should be kept in finite when we calculate the scalar-type coupling constant

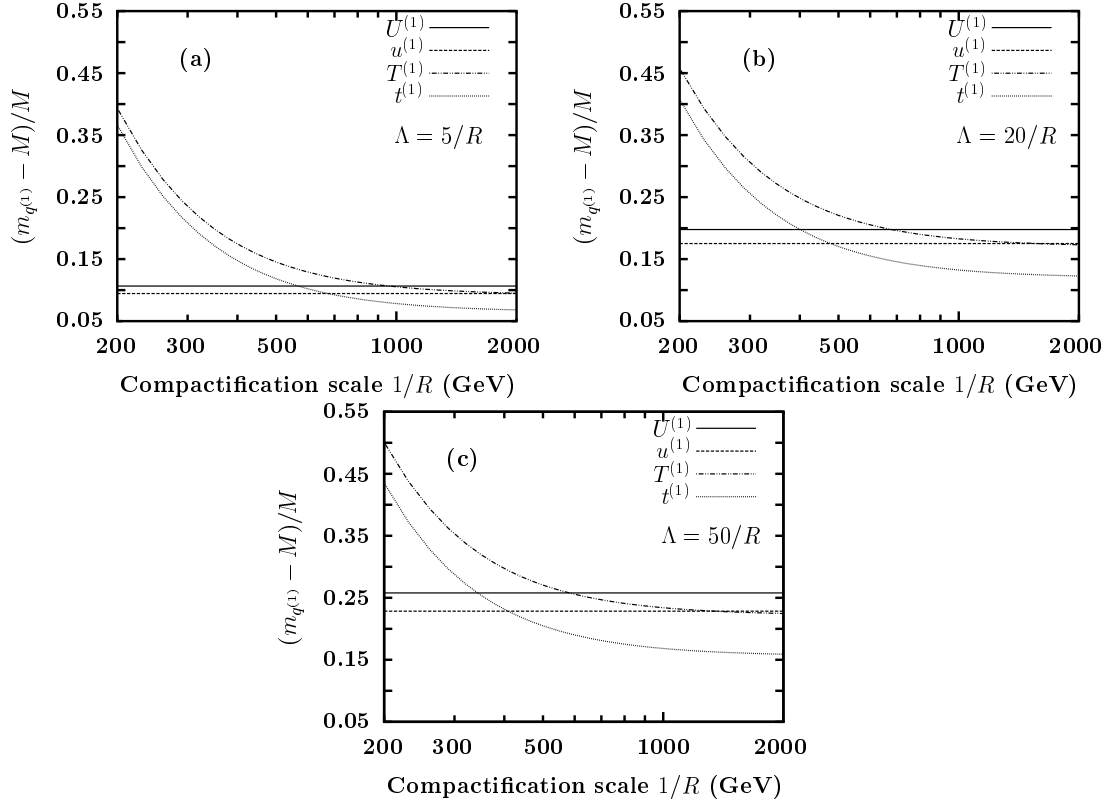


Fig. 3. Mass degeneracy between LKP dark matter and first KK quarks, $(m_{q^{(1)}} - M)/M$, for $\Lambda = 5/R$, $20/R$, and $50/R$.

f_q in Eq. (2·2), since such a type of coupling flips the chirality of the quark and the mixing is expected to contribute to the coupling.

Figure 3 shows the mass degeneracy between LKP dark matter and first KK quarks, $(m_{q^{(1)}} - M)/M$, for $q = U, u, T$, and t . We set $\Lambda = 5/R$, $20/R$, and $50/R$ for panels (a), (b), and (c), respectively. In this calculation, the gauge coupling constants are set to be the values at the electroweak scale. For a larger cutoff scale, the mass degeneracy is relaxed owing to the logarithmic factor in radiative corrections.

4.2. Scattering with light quarks and gluons

Now, we calculate the scattering amplitude of the LKP with light quarks. This process is given at the tree level. Although several authors have already evaluated the contribution,^{3), 14), 15), 35)} they mixed the contribution of twist-2-type operators with the scalar-type one and did not evaluate them correctly. The relevant Lagrangian is obtained by taking $(\psi_1, \psi_2) = (q, Q^{(1)})$ and $(q, q^{(1)})$ in Eq. (3·1). Here, $q^{(n)}$ and $Q^{(n)}$ describes the mass eigenstate of the n -th KK quarks, which are the $SU(2)_L$ singlet and doublet, respectively, and the coupling coefficients are given as (see Appendix)

$$a_{Q^{(1)}q} = -\frac{g_1}{2}(\cos \alpha^{(1)} Y_{qL} + \sin \alpha^{(1)} Y_{qR}),$$

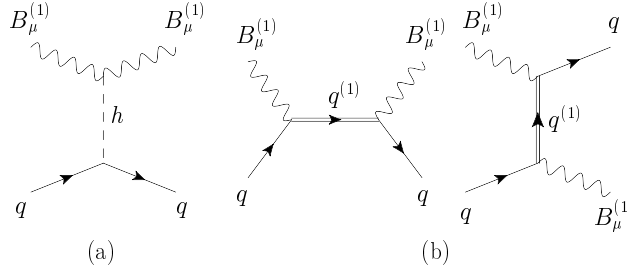


Fig. 4. Tree level diagrams for elastic scattering of $B^{(1)}$ with light quarks: (a) Higgs boson exchange contribution, and (b) KK quark exchange contributions.

$$\begin{aligned}
 b_{Q^{(1)}q} &= -\frac{g_1}{2}(-\cos\alpha^{(1)}Y_{qL} + \sin\alpha^{(1)}Y_{qR}), \\
 a_{q^{(1)}q} &= \frac{g_1}{2}(\sin\alpha^{(1)}Y_{qL} + \cos\alpha^{(1)}Y_{qR}), \\
 b_{q^{(1)}q} &= \frac{g_1}{2}(-\sin\alpha^{(1)}Y_{qL} + \cos\alpha^{(1)}Y_{qR}).
 \end{aligned} \tag{4.13}$$

In the above expression, Y_{qL} and Y_{qR} are hypercharges of left-handed and right-handed quarks, respectively. (For instance, $Y_{uL} = \frac{1}{6}$, $Y_{dR} = -\frac{1}{3}$.) The mixing angle $\alpha^{(1)}$ is defined in Eq. (4.10). Those interaction terms generate diagrams of the first KK quark exchange (Fig. 4(b)). In addition, there also exists a tree level scattering process by the standard-model Higgs boson exchange (Fig. 4(a)). In the Higgs boson exchange process, not only the standard-model Higgs boson but n -th excited KK Higgs bosons ($n \geq 2$) propagate. However, this effect is so small compared with that of the standard-model Higgs boson that we ignore the contribution.

Using the results in the previous section, we derive the coefficients of the effective Lagrangian in Eq. (2.2) as

$$\begin{aligned}
 f_q &= -\frac{g_1^2}{4m_h^2} - \frac{g_1^2}{4} \left[Y_{qL}^2 \frac{m_{Q^{(1)}}^2}{(m_{Q^{(1)}}^2 - M^2)^2} + Y_{qR}^2 \frac{m_{q^{(1)}}^2}{(m_{q^{(1)}}^2 - M^2)^2} \right] \\
 &\quad + \frac{g_1^2 Y_{qL} Y_{qR}}{m_{Q^{(1)}} + m_{q^{(1)}}} \left[\frac{m_{Q^{(1)}}}{m_{Q^{(1)}}^2 - M^2} + \frac{m_{q^{(1)}}}{m_{q^{(1)}}^2 - M^2} \right],
 \end{aligned} \tag{4.14}$$

$$d_q = \frac{ig_1^2 M}{2} \left[\frac{Y_{qL}^2}{m_{Q^{(1)}}^2 - M^2} + \frac{Y_{qR}^2}{m_{q^{(1)}}^2 - M^2} \right], \tag{4.15}$$

$$g_q = -g_1^2 M^2 \left[\frac{Y_{qL}^2}{(m_{Q^{(1)}}^2 - M^2)^2} + \frac{Y_{qR}^2}{(m_{q^{(1)}}^2 - M^2)^2} \right]. \tag{4.16}$$

The first term in Eq. (4.14) corresponds to the standard-model Higgs exchange contribution, while the other terms come from the KK quark exchange processes.

Next, let us discuss the scattering of the LKP with gluons. The contribution of this scattering process has not been taken into account or has not been properly calculated before. As we will see, however, it is not negligible. This scattering process is induced by one-loop level. The diagrams that contribute to the scattering

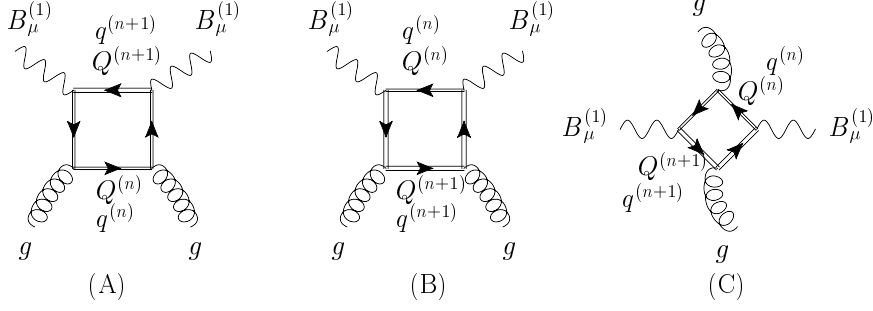


Fig. 5. One-loop diagrams for the effective interaction of $B^{(1)}$ with gluons via KK quarks. Diagram (A) gives a long-distance contribution, whereas (B) and (C) give short-distance ones.

with gluons are categorized into three types: (i) quark and the first KK quark contribution, (ii) higher KK quark contribution, and (iii) standard-model Higgs boson exchange contribution, such that

$$f_G = f_G^{(i)} + f_G^{(ii)} + f_G^{(iii)}. \quad (4.17)$$

Let us first closely look at contributions (i) and (ii). They are induced from the diagrams depicted in Fig. 5. The type (i) contribution is given by the interaction Lagrangian, which was introduced in the previous tree level calculation (*i.e.*, $(\psi_1, \psi_2) = (q, q^{(1)})$ and $(q, Q^{(1)})$). The relevant Lagrangian for the type (ii) contribution, on the other hand, is given by taking $(\psi_1, \psi_2) = (q^{(n)}, q^{(n+1)})$, $(Q^{(n)}, Q^{(n+1)})$, $(q^{(n)}, Q^{(n+1)})$, and $(Q^{(n)}, q^{(n+1)})$ ($n \geq 1$) in Eq. (3.1), with the couplings,

$$\begin{aligned} a_{q^{(n+1)}q^{(n)}} &= -\frac{g_1}{\sqrt{2}} [Y_{qL} \sin \alpha^{(n)} \sin \alpha^{(n+1)} + Y_{qR} \cos \alpha^{(n)} \cos \alpha^{(n+1)}], \\ a_{Q^{(n+1)}Q^{(n)}} &= -\frac{g_1}{\sqrt{2}} [Y_{qL} \cos \alpha^{(n)} \cos \alpha^{(n+1)} + Y_{qR} \sin \alpha^{(n)} \sin \alpha^{(n+1)}], \\ b_{Q^{(n+1)}q^{(n)}} &= -\frac{g_1}{\sqrt{2}} [Y_{qL} \sin \alpha^{(n)} \cos \alpha^{(n+1)} - Y_{qR} \cos \alpha^{(n)} \sin \alpha^{(n+1)}], \\ b_{q^{(n+1)}Q^{(n)}} &= -\frac{g_1}{\sqrt{2}} [Y_{qL} \cos \alpha^{(n)} \sin \alpha^{(n+1)} - Y_{qR} \sin \alpha^{(n)} \cos \alpha^{(n+1)}], \\ b_{q^{(n+1)}q^{(n)}} &= b_{Q^{(n+1)}Q^{(n)}} = a_{Q^{(n+1)}q^{(n)}} = a_{q^{(n+1)}Q^{(n)}} = 0. \end{aligned} \quad (4.18)$$

(For the derivation, see Appendix.)

As we discussed in §3, there exists the long-distance contribution when the quark runs in the loop. This is the case for the type (i) contribution. Thus, in the calculation of the type (i) contribution, the diagrams in which light quarks run in the loop should not be included. Then, the contribution to the scalar effective coupling to the gluon is written as

$$\begin{aligned} f_G^{(i)} &= \frac{\alpha_s}{4\pi} \sum_{q=c,b,t} c_q \left[(a_{Q^{(1)}q}^2 + b_{Q^{(1)}q}^2) f_+^{(A)}(M; m_q, m_{Q^{(1)}}) + (a_{Q^{(1)}q}^2 - b_{Q^{(1)}q}^2) f_-^{(A)}(M; m_q, m_{Q^{(1)}}) \right. \\ &\quad \left. + (a_{q^{(1)}q}^2 + b_{q^{(1)}q}^2) f_+^{(A)}(M; m_q, m_{q^{(1)}}) + (a_{q^{(1)}q}^2 - b_{q^{(1)}q}^2) f_-^{(A)}(M; m_q, m_{q^{(1)}}) \right] \end{aligned}$$

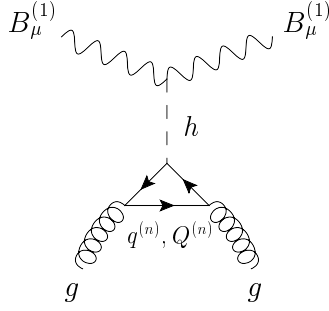


Fig. 6. One-loop diagram for the effective interaction of $B^{(1)}$ with gluons through the exchange of standard-model Higgs boson.

$$\begin{aligned}
& + \frac{\alpha_s}{4\pi} \sum_{q=\text{all}} \sum_{I=\text{B,C}} \left[(a_{Q^{(1)}q}^2 + b_{Q^{(1)}q}^2) f_+^{(I)}(M; m_q, m_{Q^{(1)}}) + (a_{Q^{(1)}q}^2 - b_{Q^{(1)}q}^2) f_-^{(I)}(M; m_q, m_{Q^{(1)}}) \right. \\
& \quad \left. + (a_{q^{(1)}q}^2 + b_{q^{(1)}q}^2) f_+^{(I)}(M; m_q, m_{q^{(1)}}) + (a_{q^{(1)}q}^2 - b_{q^{(1)}q}^2) f_-^{(I)}(M; m_q, m_{q^{(1)}}) \right].
\end{aligned} \tag{4.19}$$

On the other hand, for the type (ii) contribution, all the diagrams are short-distance contributions. Then,

$$\begin{aligned}
f_G^{(ii)} = \frac{\alpha_s}{4\pi} \sum_{q=\text{all}} \sum_{I=\text{A,B,C}} & \left\{ a_{q^{(n+1)}q^{(n)}}^2 [f_+^{(I)}(M; m_{q^{(n)}}, m_{q^{(n+1)}}) + f_-^{(I)}(M; m_{q^{(n)}}, m_{q^{(n+1)}})] \right. \\
& + a_{Q^{(n+1)}Q^{(n)}}^2 [f_+^{(I)}(M; m_{Q^{(n)}}, m_{Q^{(n+1)}}) + f_-^{(I)}(M; m_{Q^{(n)}}, m_{Q^{(n+1)}})] \\
& + b_{Q^{(n+1)}q^{(n)}}^2 [f_+^{(I)}(M; m_{q^{(n)}}, m_{Q^{(n+1)}}) - f_-^{(I)}(M; m_{q^{(n)}}, m_{Q^{(n+1)}})] \\
& \left. + b_{q^{(n+1)}Q^{(n)}}^2 [f_+^{(I)}(M; m_{Q^{(n)}}, m_{q^{(n+1)}}) - f_-^{(I)}(M; m_{Q^{(n)}}, m_{q^{(n+1)}})] \right\}.
\end{aligned} \tag{4.20}$$

Finally, we discuss the type (iii) contribution. The standard-model Higgs boson is coupled with the standard-model quarks and also higher KK quarks, and then the triangle loop diagrams of heavy quarks and KK quarks contribute to the effective scalar coupling to gluons. The corresponding diagram is shown in Fig. 6. In the triangle loop, all the higher KK quarks run in the loop, in addition to heavy quarks. Then, we obtain the standard-model Higgs exchange contribution as

$$\begin{aligned}
f_G^{(iii)} & = \frac{g_1^2 \alpha_s}{48\pi m_h^2} \left[(c_c + c_b + c_t) + m_t c_t \sum_n \sin 2\alpha^{(n)} \left(\frac{1}{m_{t^{(n)}}} + \frac{1}{m_{T^{(n)}}} \right) \right] \\
& = \frac{g_1^2 \alpha_s}{48\pi m_h^2} \left[(c_c + c_b + c_t) + c_t \sum_n \frac{2m_t^2}{m_{t^{(n)}} m_{T^{(n)}}} \right].
\end{aligned} \tag{4.21}$$

In this calculation, we ignore quark masses except that of the top quark.

4.3. Results

Now, we are at the point of showing the numerical results of the cross section. At the beginning, let us examine the case in which n -th KK modes with $n \geq 2$ are neglected so that we see features of the cross section. Also, it is worthwhile when one applies the formulae for other vector dark matter scenarios. In Fig. 7, the spin-independent cross section of the LKP with a proton (σ_{SI}) is depicted. Here, we set $m_{q^{(1)}} = m_{Q^{(1)}} \equiv m_{1\text{st}}$ for simplicity, except for the masses of the first KK top quarks, for which we take $m_{t^{(1)}}^2 = m_{T^{(1)}}^2 = m_{1\text{st}}^2 + m_t^2$ (m_t is top quark mass), and show the contours of the cross section on the plane, the LKP mass vs the mass degeneracy between the first excited KK quarks and the LKP, $(m_{1\text{st}} - M)/M$. The standard-model Higgs boson mass is set as $m_h = 120$ GeV, 200 GeV, and 500 GeV. From the figure, it is found that the cross section is enhanced when the first KK quark and LKP masses are degenerate, as is expected. Such a behavior was already discussed in the previous works. However, with the complete calculation that has been carried out here, we have discovered that the spin-independent cross section is larger than the former theoretical predictions. In the case of $m_h = 120$ GeV and the mass degeneracy of 10%, for instance, the cross section ranges from 3.5×10^{-43} cm² to 1.3×10^{-46} cm² when the LKP mass is from 200 GeV to 1 TeV. This result is larger than those in the previous works^{3), 14), 15)} up to about a factor of ten. In our calculation, we have found that the twist-2-type operator contribution, which had not been taken into account correctly in the previous works, dominates the effective coupling when $M \lesssim O(\text{TeV})$ and enhances the cross section. In the parameter region $M \gtrsim O(\text{TeV})$, on the other hand, the standard-model Higgs boson contribution (from both tree- and one-loop-level diagrams) dominates the effective coupling. Then, the cross section is determined using the standard-model Higgs boson mass in the parameter region.

To clarify the behavior of the cross section, we also plot each contribution in the effective coupling f_N in Fig. 8. Here, we set $m_h = 120$ GeV and 10% of the mass degeneracy. In the figure, “scalar”, “twist-2”, and “gluon” correspond to the first, second, and third terms in Eq. (2.9) (except for the standard-model Higgs exchange contribution), respectively, and the standard-model Higgs exchange contribution (including tree and one-loop levels) is denoted as “Higgs”. We have found that all the contributions have the same (negative) sign so that they are constructive. As a consequence, the cross section is enhanced in a wide parameter region. In the figure, it is seen that the twist-2 contribution dominates the effective coupling when $M \lesssim O(\text{TeV})$. The gluon contribution is subleading, but not negligible at all. On the other hand, the standard-model Higgs boson contribution dominates the effective coupling when $M \gtrsim O(\text{TeV})$.

For completeness, we show the spin-dependent scattering cross section. The spin-dependent interaction is generated by KK quark exchange at the tree level, and it is found that the cross section is enhanced when the first KK quark and LKP masses are degenerate as expected from Eq. (3.3). In Fig. 9, the spin-dependent scattering cross section with a proton is shown as a function of the LKP mass assuming the degeneracies are 10%, 20%, and 25%. We found that the spin-dependent scattering

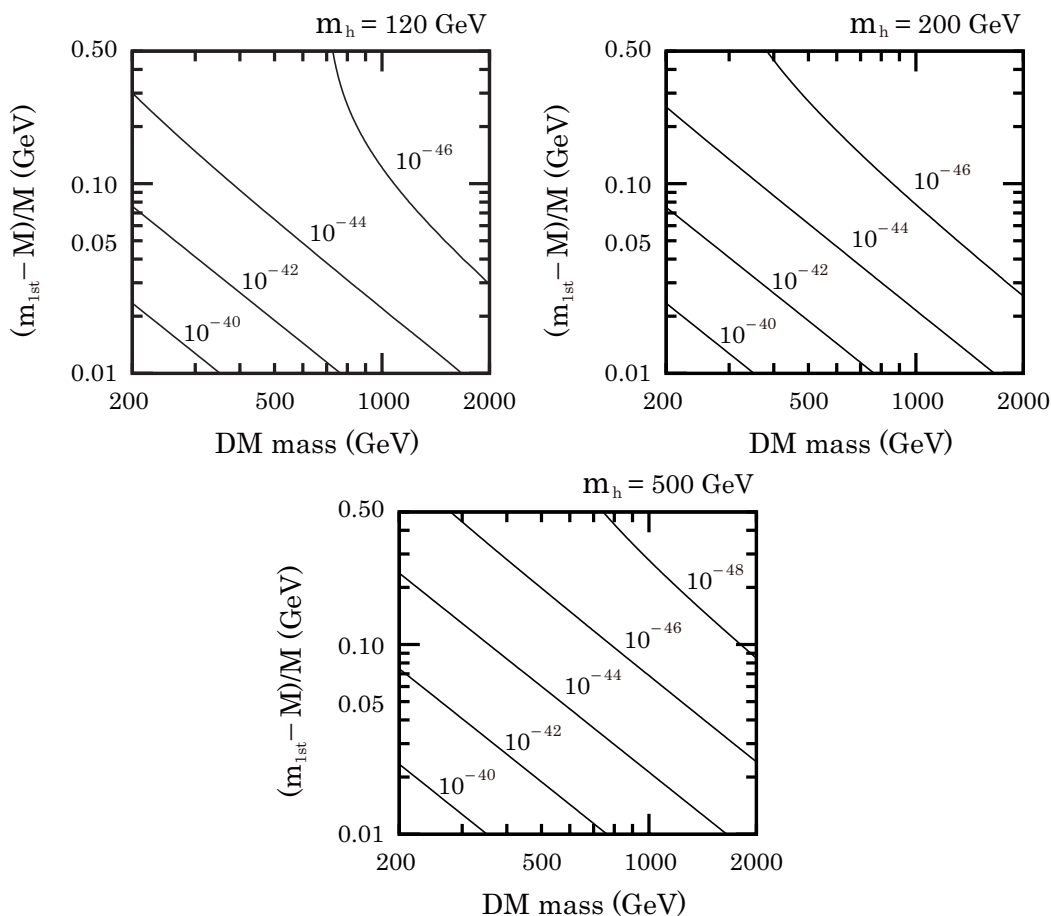


Fig. 7. Spin-independent cross section with a proton on the plane, LKP mass vs. mass degeneracy $(m_{1st} - M)/M$. Here, we take $m_h = 120$ GeV (upper left), 200 GeV (upper right), and 500 GeV (bottom). Lines correspond to the contours $\sigma_{SI} = 10^{-40}$ cm², 10^{-42} cm², 10^{-44} cm², 10^{-46} cm², and 10^{-48} cm² from bottom to top.

cross section is consistent with Refs.^{3),14),15)}

Next, we discuss a more realistic situation for the direct detection of the LKP dark matter in the MUED model, including higher KK mode contributions. For the cutoff scale $\Lambda = n/R$, the KK particles up to the n -th mode are included in the calculations. Furthermore, we employ the radiative corrections for the spectra of KK particles discussed in §4.1. To see the importance of the higher KK mode contribution, we show the cutoff dependence of the spin-independent cross section with a proton by taking $\Lambda = 5/R$, $20/R$, and $50/R$ in Fig. 10. In the figure, we take $m_h = 120$ GeV. For a larger cutoff scale, although a larger number of KK modes could contribute to the cross section, the cross section tends to be smaller than that for the smaller cutoff scale. This is because the large cutoff scale makes the mass degeneracy relax owing to the radiative corrections (as shown in Fig. 3), and this reductive effect dominates over the increasing effect from higher KK mode

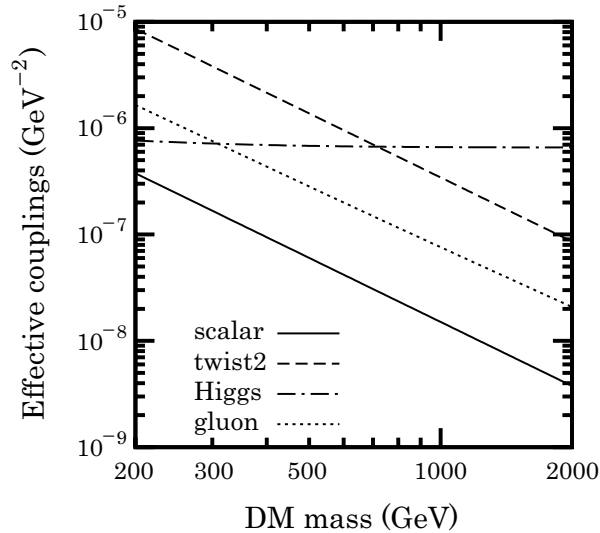


Fig. 8. Each contribution in effective coupling f_N/m_N given in Eq. (2.9). Here, we set $m_h = 120$ GeV and $(m_{1st} - M)/M = 0.1$. “scalar”, “twist-2”, and “gluon” correspond to the first, second, and third terms in Eq. (2.9) (except for standard-model Higgs exchange contribution), respectively, and standard-model Higgs exchange contribution, including tree and one-loop levels, is denoted as “Higgs”.

contributions.

Finally, we discuss the feasibility of the direct detection of KK photon dark matter for the parameter space in which its relic abundance can be reproduced in accordance with the WMAP result. We plot the relationship between the spin-independent scattering cross section with a proton and the relic abundance in Fig. 11. The charged Higgs boson is the LKP in the upper right region, and hence this region is excluded. The dark (light) gray region shows the 1σ (2σ) allowed region from the WMAP observational result, which is the result calculated in Ref.²⁸⁾ Each line corresponds to the spin-independent cross section $\sigma_{SI} = 10^{-45}$ cm², 3×10^{-46} cm², 10^{-46} cm², 4×10^{-47} cm², and 10^{-47} cm². The spin-independent cross section ranges from about 3×10^{-46} cm² to 5×10^{-48} cm² on the allowed region of the relic abundance, and are just below the present experimental bounds. The ongoing and future experiments for the direct detection of dark matter would reach sensitivities in this range.

§5. Conclusions

In this paper, we assume that WIMP dark matter is composed of vector particles and have evaluated an elastic cross section with nucleons in the direct detection experiments. The vector dark matter is predicted in models beyond the standard model, such as the KK photon in the UED model and the T -odd heavy photon in the Littlest Higgs model with T -parity. On the other hand, however, the cross section had not yet been consistently evaluated, even at the leading order of α_s . We have

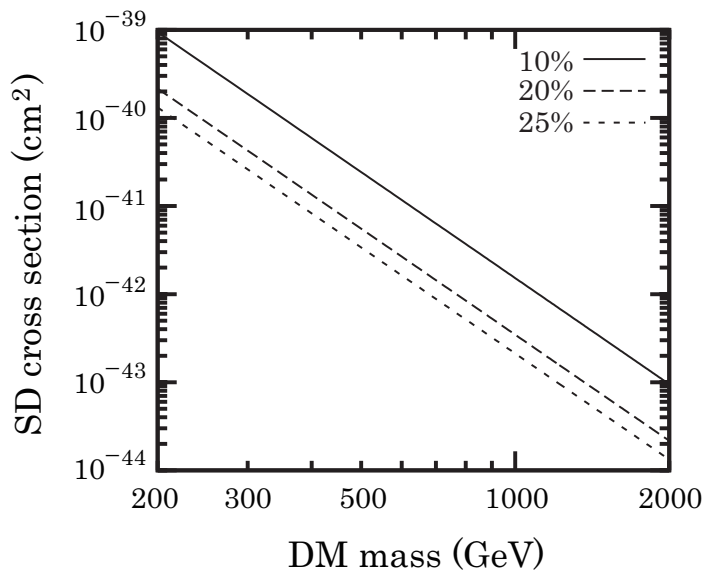


Fig. 9. Spin-dependent cross section with a proton. Here, we set $(m_{1st} - M)/M = 0.1, 0.2,$ and 0.25 from top to bottom.

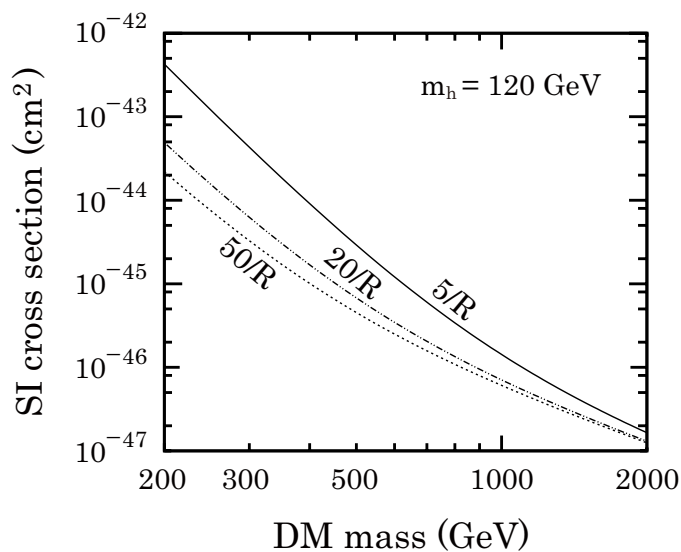


Fig. 10. Spin-independent cross section with a proton for $m_h = 120\text{GeV}$. Each line corresponds to $\Lambda = 5/R, 20/R,$ and $50/R,$ respectively.

derived the general formulae for the cross section of general vector dark matter with nucleons.

As an application of our formulae, we discussed the direct detection of the first KK photon in the MUED model. We found that the cross section is larger than those in the previous works by up to a factor of 10. We showed that the spin-independent

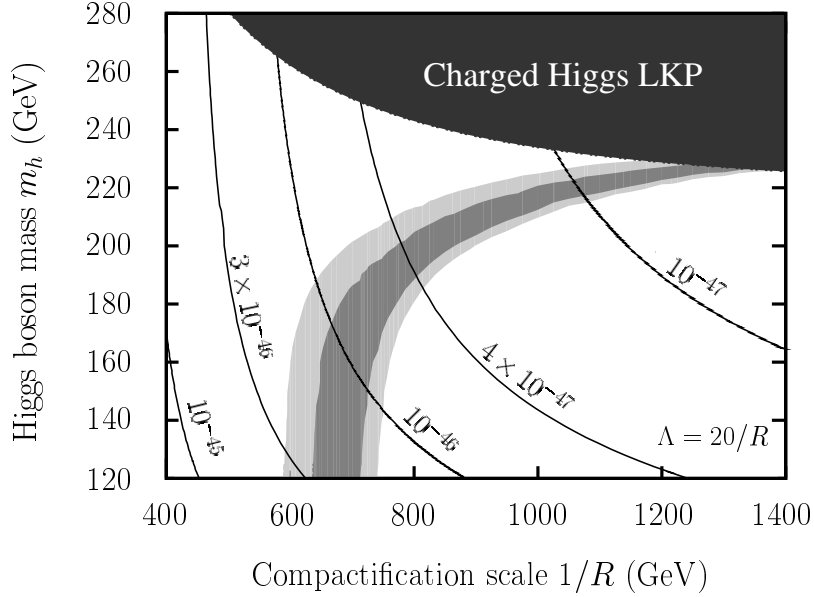


Fig. 11. Contour plot of relic abundance consistent with WMAP result and spin-independent cross section in the $(1/R, m_h)$ plane for $\Lambda = 20/R$. The dark (light) gray region shows the 1σ (2σ) allowed region in light of relic abundance. Each line corresponds to a spin-independent scattering cross section with a proton $\sigma_{\text{SI}} = 10^{-45} \text{ cm}^2$, $3 \times 10^{-46} \text{ cm}^2$, 10^{-46} cm^2 , $4 \times 10^{-47} \text{ cm}^2$, and 10^{-47} cm^2 .

cross section of the KK photon with a proton ranges from nearly $3 \times 10^{-46} \text{ cm}^2$ to $5 \times 10^{-48} \text{ cm}^2$ on the parameter region with the thermal relic abundance consistent with the cosmological observations. The future direct detection experiments with ton-scale detectors might cover the range.

Note Added: While preparing the manuscript, we became aware of a paper by G. Belanger, M. Kakizaki and A. Pukhov.³⁶⁾ In that paper, the elastic cross section of the KK photon with nucleons in the MUED model was calculated using microOMEGA.³⁷⁾ In the calculation, the tree level contribution was included in the scattering process whereas the one-loop contributions were incomplete.

§6. Acknowledgments

We thank Alexander Pukhov for pointing out errors in Eqs. (3-16) and (3-18) in the previous versions of this paper. The work was supported in part by Grants-in-Aid from the Ministry of Education, Culture, Sports, Science and Technology (MEXT), Government of Japan, No. 20244037, No. 2054252, and No. 2244021 (J.H.). The work of J.H. is also supported by the World Premier International Research Center Initiative (WPI Initiative), MEXT, Japan. This work was also supported in part by the U.S. Department of Energy under contract No. DE-FG02-92ER40701, and by the Gordon and Betty Moore Foundation (K.I.).

Appendix A

— Relevant Feynman rules —

In this Appendix, we collect parts of the Lagrangian in the MUED model.

- Standard-model Higgs boson coupling with the first KK particle of $U(1)_Y$ gauge boson

$$\mathcal{L}_{BBh^0} = \frac{1}{4}g_1^2 v h^0 B_\mu^{(1)} B^{(1)\mu} \quad (\text{A}\cdot 1)$$

- Standard-model Higgs boson coupling with n -th KK quarks

$$\begin{aligned} \mathcal{L}_{q^{(n)}q^{(n)}h^0} = & -\frac{m_q}{v}h^0 \sum_{n=1} \left[\sin 2\alpha^{(n)} (\bar{Q}^{(n)} Q^{(n)} + \bar{q}^{(n)} q^{(n)}) \right. \\ & \left. + \cos 2\alpha^{(n)} (\bar{q}^{(n)} \gamma_5 Q^{(n)} - \bar{Q}^{(n)} \gamma_5 q^{(n)}) \right] \end{aligned} \quad (\text{A}\cdot 2)$$

- Coupling of the first KK particle of the $U(1)_Y$ gauge boson with the first KK quarks and quarks

$$\begin{aligned} \mathcal{L}_{q^{(n)}qB} = & -g_1 \bar{q} \gamma^\mu [\cos \alpha^{(1)} Y_{qL} P_L + \sin \alpha^{(1)} Y_{qR} P_R] Q^{(1)} B_\mu^{(1)} \\ & -g_1 \bar{Q}^{(1)} \gamma^\mu [\cos \alpha^{(1)} Y_{qL} P_L + \sin \alpha^{(1)} Y_{qR} P_R] q B_\mu^{(1)} \\ & +g_1 \bar{q} \gamma^\mu [\sin \alpha^{(1)} Y_{qL} P_L + \cos \alpha^{(1)} Y_{qR} P_R] q^{(1)} B_\mu^{(1)} \\ & +g_1 \bar{Q}^{(1)} \gamma^\mu [\sin \alpha^{(1)} Y_{qL} P_L + \cos \alpha^{(1)} Y_{qR} P_R] q B_\mu^{(1)} \end{aligned} \quad (\text{A}\cdot 3)$$

- Coupling of the first KK particle of the $U(1)_Y$ gauge boson with the n -th and $(n+1)$ -th KK quarks

$$\begin{aligned} \mathcal{L}_{q^{(n)}q^{(n+1)}B} = & -\frac{g_1}{\sqrt{2}} B_\mu^{(1)} \sum_{n=1} [(Y_{qL} \sin \alpha^{(n)} \sin \alpha^{(n+1)} + Y_{qR} \cos \alpha^{(n)} \cos \alpha^{(n+1)}) \\ & \times (\bar{q}^{(n+1)} \gamma^\mu q^{(n)} + \bar{q}^{(n)} \gamma^\mu q^{(n+1)}) \\ & + (Y_{qL} \cos \alpha^{(n)} \cos \alpha^{(n+1)} + Y_{qR} \sin \alpha^{(n)} \sin \alpha^{(n+1)}) \\ & \times (\bar{Q}^{(n+1)} \gamma^\mu Q^{(n)} + \bar{Q}^{(n)} \gamma^\mu Q^{(n+1)}) \\ & + (Y_{qL} \sin \alpha^{(n)} \cos \alpha^{(n+1)} - Y_{qR} \cos \alpha^{(n)} \sin \alpha^{(n+1)}) \\ & \times (\bar{Q}^{(n+1)} \gamma^\mu \gamma_5 q^{(n)} + \bar{q}^{(n)} \gamma^\mu \gamma_5 Q^{(n+1)}) \\ & + (Y_{qL} \cos \alpha^{(n)} \sin \alpha^{(n+1)} - Y_{qR} \sin \alpha^{(n)} \cos \alpha^{(n+1)}) \\ & \times (\bar{q}^{(n+1)} \gamma^\mu \gamma_5 Q^{(n)} + \bar{Q}^{(n)} \gamma^\mu \gamma_5 q^{(n+1)})] \end{aligned} \quad (\text{A}\cdot 4)$$

References

- 1) G. Hinshaw *et al.* [WMAP Collaboration], *Astrophys. J. Suppl.* **180** (2009), 225.
- 2) G. Servant and T. M. P. Tait, *Nucl. Phys. B* **650** (2003), 391.
- 3) H. C. P. Cheng, J. L. Feng and K. T. Matchev, *Phys. Rev. Lett.* **89** (2002), 211301.
- 4) T. Appelquist, H. C. Cheng and B. A. Dobrescu, *Phys. Rev. D* **64** (2001), 035002.

- 5) H. C. Cheng, K. T. Matchev and M. Schmaltz, *Phys. Rev. D* **66** (2002), 036005.
- 6) J. Hubisz and P. Meade, *Phys. Rev. D* **71** (2005), 035016.
- 7) A. Birkedal, A. Noble, M. Perelstein and A. Spray, *Phys. Rev. D* **74** (2006), 035002.
- 8) M. Asano, S. Matsumoto, N. Okada and Y. Okada, *Phys. Rev. D* **75** (2007), 063506.
- 9) N. Arkani-Hamed, A. G. Cohen and H. Georgi, *Phys. Lett. B* **513** (2001), 232; N. Arkani-Hamed, A. G. Cohen, E. Katz, A. E. Nelson, T. Gregoire and J. G. Wacker, *JHEP* **0208** (2002), 021; N. Arkani-Hamed, A. G. Cohen, E. Katz and A. E. Nelson, *JHEP* **0207** (2002), 034.
- 10) H. C. Cheng and I. Low, *JHEP* **0408** (2004), 061; I. Low, *JHEP* **0410** (2004), 067;
- 11) E. Aprile *et al.* [XENON100 Collaboration], arXiv:1104.2549 [astro-ph.CO].
- 12) J. Hisano, K. Ishiwata and N. Nagata, *Phys. Lett. B* **690** (2010), 311.
- 13) J. Hisano, K. Ishiwata and N. Nagata, *Phys. Rev. D* **82** (2010), 115007.
- 14) G. Servant and T. M. P. Tait, *New J. Phys.* **4** (2002), 99.
- 15) S. Arrenberg, L. Baudis, K. Kong, K. T. Matchev and J. Yoo, *Phys. Rev. D* **78** (2008), 056002.
- 16) M. Drees and M. Nojiri, *Phys. Rev. D* **48** (1993), 3483.
- 17) H. D. Politzer, *Nucl. Phys. B* **172** (1980), 349.
- 18) A. Corsetti and P. Nath, *Phys. Rev. D* **64** (2001), 125010. [arXiv:hep-ph/0003186].
- 19) H. Ohki *et al.*, *Phys. Rev. D* **78** (2008), 054502.
- 20) H. Y. Cheng, *Phys. Lett. B* **219** (1989), 347.
- 21) D. Adams *et al.* [Spin Muon Collaboration], *Phys. Lett. B* **357** (1995), 248.
- 22) J. Pumplin, D. R. Stump, J. Huston, H. L. Lai, P. M. Nadolsky and W. K. Tung, *JHEP* **0207** (2002), 012.
- 23) M. A. Shifman, A. I. Vainshtein and V. I. Zakharov, *Phys. Lett. B* **78** (1978), 443.
- 24) A. Djouadi and M. Drees, *Phys. Lett. B* **484** (2000), 183.
- 25) M. Kakizaki, S. Matsumoto, Y. Sato and M. Senami, *Phys. Rev. D* **71** (2005), 123522.
- 26) F. Burnell and G. D. Kribs, *Phys. Rev. D* **73** (2006), 015001.
- 27) K. Kong and K. T. Matchev, *JHEP* **0601** (2006), 038.
- 28) M. Kakizaki, S. Matsumoto and M. Senami, *Phys. Rev. D* **74** (2006), 023504.
- 29) K. Agashe, N. G. Deshpande and G. H. Wu, *Phys. Lett. B* **514** (2001), 309.
- 30) A. J. Buras, A. Poschenrieder, M. Spranger and A. Weiler, *Nucl. Phys. B* **678** (2004), 455.
- 31) U. Haisch and A. Weiler, *Phys. Rev. D* **76** (2007), 034014.
- 32) V. Bashiry and K. Zeynali, *Phys. Rev. D* **79** (2009), 033006.
- 33) D. Chakraverty, K. Huitu and A. Kundu, *Phys. Lett. B* **558** (2003), 173.
- 34) I. Gogoladze and C. Macesanu, *Phys. Rev. D* **74** (2006), 093012.
- 35) V. K. Oikonomou, J. D. Vergados, C. C. Moustakidis, *Nucl. Phys.* **B773** (2007), 19-42.
- 36) G. Belanger, M. Kakizaki and A. Pukhov, arXiv:1012.2577 [hep-ph].
- 37) G. Belanger, F. Boudjema, A. Pukhov and A. Semenov, *Comput. Phys. Commun.* **176** (2007), 367.